Journal of Geophysical Research: Oceans

RESEARCH ARTICLE
10.1029/2017JC013657

Annual and Semiannual Cycles of Diurnal Warming of Sea Surface Temperature in the South China Sea

Yunwei Yan[1], Guihua Wang[2], Changlin Chen[2], and Zheng Ling[3]

[1]State Key Laboratory of Satellite Ocean Environment Dynamics, Second Institute of Oceanography, State Oceanic Administration, Hangzhou, China, [2]Department of Atmospheric and Oceanic Sciences & Institute of Atmospheric Sciences, Fudan University, Shanghai, China, [3]Guangdong Key Laboratory of Coastal Ocean Variability and Disaster Prediction, Guangdong Ocean University, Zhanjiang, China

Key Points:
- Annual cycle of diurnal warming is relatively large in the whole SCS, while semiannual cycle increases from north to south
- Annual (semiannual) cycle of wind speed is the most important factor for the annual (semiannual) cycle of diurnal warming
- Annual and semiannual cycles demonstrate robust mesoscale features in the lees of hills/islands as a result of sheltering from the monsoon

Correspondence to:
C. Chen,
chencl@fudan.edu.cn

Citation:
Yan, Y., Wang, G., Chen, C., & Ling, Z. (2018). Annual and semiannual cycles of diurnal warming of sea surface temperature in the South China Sea. *Journal of Geophysical Research: Oceans*, *123*, 5797–5807. https://doi.org/10.1029/2017JC013657

Received 29 NOV 2017
Accepted 30 JUL 2018
Accepted article online 6 AUG 2018
Published online 19 AUG 2018

Abstract Based on the SeaFlux data set, an empirical parameterization, and a one-dimensional ocean mixed-layer model, the annual and semiannual cycles of diurnal warming of sea surface temperature (dSST) in the South China Sea (SCS) are examined. The amplitude of the annual cycle is greater than 0.1 °C, and the annual cycle reaches its maxima in April/May/June in most areas of the SCS, while the amplitude of the semiannual cycle of dSST increases from north to south with the month of its maxima changing from February to March along a northwest-southeast axis. Relative to the amplitude of the annual cycle of dSST, the semiannual cycle is of much smaller amplitude north of 17°N, but of comparable or larger amplitude south of 17°N. The annual (semiannual) cycle of wind speed is the most important factor for the annual (semiannual) cycle of dSST. The annual (semiannual) cycle of wind speed drives the annual (semiannual) cycle of dSST primarily by influencing oceanic vertical turbulent mixing. Aside from these basin-scale features, the dSST annual and semiannual cycles demonstrate robust mesoscale features in the lees of hills/islands as a result of sheltering from the monsoon.

Plain Language Summary Based on the SeaFlux data set, an empirical parameterization, and a one-dimensional ocean mixed-layer model, the annual and semiannual cycles of diurnal warming of sea surface temperature (dSST) in the South China Sea are examined. The annual cycle of diurnal warming is relatively large in the whole South China Sea, while semiannual cycle increases from north to south. Relative to the amplitude of the annual cycle of dSST, the semiannual cycle is of much smaller amplitude north of 17°N, but of comparable or larger amplitude south of 17°N. Aside from these basin-scale features, the dSST annual and semiannual cycles demonstrate robust mesoscale features in the lees of hills/islands. The annual (semiannual) cycle of wind speed is the most important factor for the annual (semiannual) cycle of dSST. The annual (semiannual) cycle of wind speed drives the annual (semiannual) cycle of dSST primarily by influencing oceanic vertical turbulent mixing.

1. Introduction

Diurnal warming of the upper ocean is caused by the daytime absorption of solar radiation. It has a significant influence on both air-sea heat and gas fluxes (e.g., Clayson & Bogdanoff, 2013; Kettle et al., 2009; Marullo et al., 2016; Ward, 2006; Weihs & Bourassa, 2014) and sea surface temperature (SST) at longer time scales (e.g., Bernie et al., 2005, 2008; Guemas et al., 2011; Shinoda et al., 1998). While the typical magnitude of diurnal warming of SST (dSST) is O(0.1 °C; e.g., Kennedy et al., 2007; Stuart-Menteth et al., 2003), it may reach 5–7 °C on days with low wind speed and strong insolation (e.g., Gentemann et al., 2008; Gentemann & Minnett, 2008). Lower wind speed induces a larger dSST response due to weaker wind-induced turbulent mixing and reduced heat loss to the atmosphere, while stronger insolation causes larger dSST due to more heat absorption (Kawai & Wada, 2007).

The South China Sea (SCS, 99–120°E and 0–25°N) is the largest marginal sea of the northwestern Pacific Ocean. As expected, dSST can also modulate the SCS air-sea heat flux and mixed layer depth and hence SST (Clayson & Bogdanoff, 2013; Li et al., 2013). Thus, dSST is important in the SCS. Under the influence of the East Asian monsoon, dSST in the SCS exhibits large temporal variability and spatial heterogeneity (e.g., Kawai & Kawamura, 2005; Lin et al., 2011; Tu et al., 2015, 2016; Yan et al., 2014). For example, Tu et al. (2015) pointed out that dSST in the SCS exhibits obvious seasonal variation, with it being smallest during

the strong northeast winter monsoon and largest during the northeast to southwest monsoon transition. Yan et al. (2014) found that dSST is relatively large off the coast of northeastern Vietnam (in the lee of a hill) during the southwest summer monsoon because of sheltering from the monsoon. These results suggest that wind forcing has a significant impact on dSST in the SCS.

Previous studies have demonstrated that the semiannually reversing East Asian monsoon leads to an obvious semiannual signal in wind speed over the SCS (e.g., Lv et al., 2012; Xie et al., 2003). Results of harmonic analysis of the wind speed records show that the amplitude of the semiannual cycle is comparable to or even greater than that of the annual cycle, especially over the southern SCS (figure is not shown). In addition, the annual and semiannual cycles of wind speed show robust mesoscale features in the lees of hills/islands. The natural question is as follows: Does dSST also have a significant semiannual signal due to the semiannual signal of wind speed in the SCS? If yes, what is the relative importance of the annual and semiannual cycles of dSST? Do the annual and semiannual cycles have mesoscale features in the lees of hills/islands? In this study, we first examine the annual and semiannual cycles of dSST in the SCS, and then investigate the mechanisms driving these signals. Finally, the mesoscale features of the dSST annual and semiannual cycles in the lees of hills/islands are discussed.

2. Data and Method

2.1. SeaFlux dSST

In this study, dSST was derived from the SeaFlux version 1.0 (SeaFlux-V1.0) data product developed and maintained through the international SeaFlux project. The SeaFlux-V1.0 dSST is based on the *Bogdanoff and Clayson* parameterization (Clayson & Bogdanoff, 2013), which is an updated version of the Webster et al. (1996; W96 hereafter) parameterization. The data product covers the period 1998–2007 with a spatial resolution 0.25° × 0.25°.

To assess the SeaFlux-V1.0 derived dSST, three ATLAS buoys in the SCS deployed during the SCS monsoon experiment (Lau et al., 2000) were applied for comparison (Figure 1). The mean differences of dSST between the SeaFlux product and ATLAS observations were −0.05, 0.01, and −0.02 °C with root-mean-square errors of 0.07, 0.06, and 0.07 °C and correlation coefficients of 0.93, 0.94, and 0.92 (Table 1), which demonstrates that the product is capable of reproducing seasonal variation of dSST in the SCS.

2.2. W96 Parameterization

The W96 parameterization was developed based on results from a one-dimensional mixed layer ocean model, and it has been used to study dSST in the tropics (e.g., Clayson & Curry, 1996; Clayson & Weitlich, 2005, 2007). The W96 parameterization has the following form:

$$\mathrm{dSST} = a(\mathrm{PS}) + b(P) + c\ln(U) + d(\mathrm{PS})\ln(U) + e(U) + f$$

where PS is the peak solar insolation (W/m^2), P is the daily averaged precipitation (mm/hr), U is the daily averaged 10-m wind speed (m/s), and a, b, c, d, e, and f are regression coefficients as in the W96 parameterization. The terms associated with ln(U) and U represent the effects of wind-induced oceanic mixing and surface heat flux on dSST, respectively (Webster et al., 1996). The term d(PS) ln (U) means that wind-induced oceanic mixing induces a lager decrease in dSST when solar insolation is larger, possibly due to larger temperature difference across the base of the mixed layer.

To evaluate the relative importance of the annual cycles of solar radiation, wind speed, and precipitation to the annual cycle of dSST, a control run and three sensitivity runs were designed with the W96 parameterization. In the control run, the daily peak solar radiation, the daily averaged precipitation, and the daily averaged 10-m wind speed were used. The estimated dSST in the control run agreed well with ATLAS buoy observations in the SCS (Figure 1 and Table 1). In the three sensitivity runs, we first removed the annual cycles of the time series of the daily peak solar radiation, the daily averaged precipitation, and the daily averaged 10-m wind speed, respectively, and then estimated dSST. The difference of dSST in the control run and each sensitivity run was calculated to estimate the contribution of the annual cycle of solar radiation, wind speed, or precipitation. Here we define the percentage contributions as the ratio of the individual contributions of the annual cycles of solar radiation, wind speed, and precipitation relative to the sum of all three contributions. The contributions for the semiannual cycle of dSST were also examined in a similar manner.

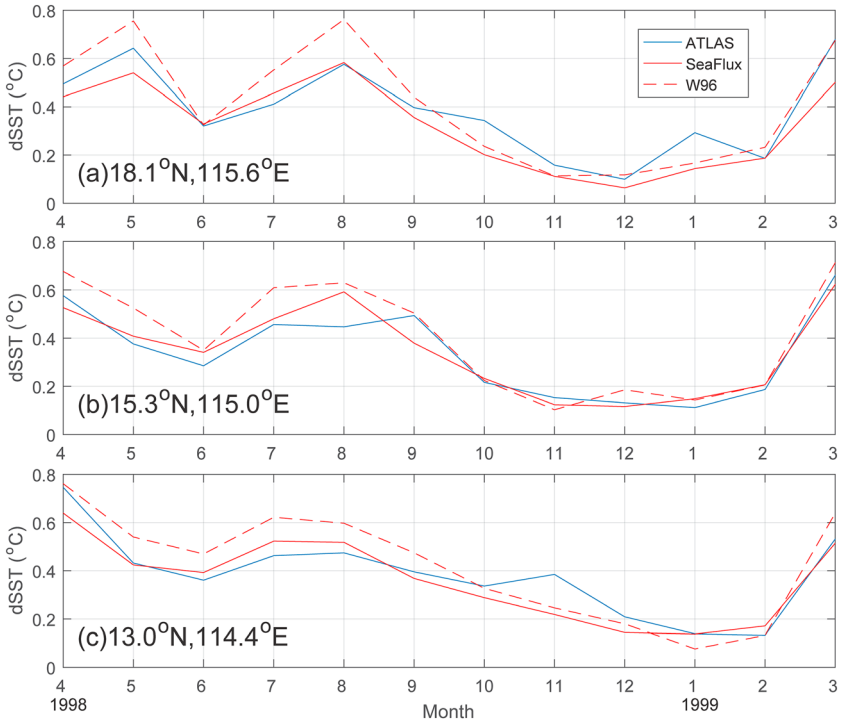

Figure 1. Monthly mean diurnal warming of sea surface temperature (dSST, °C) at (a) 18.1°N, 115.6°E, (b) 15.3°N, 115.0°E, and (c) 13.0°N, 114.4°E during the period from April 1998 to March 1999 derived from the ATLAS buoys (blue curves), the SeaFlux data set (solid red curves), and the W96 parameterization (dashed red curves).

In these calculations, the peak solar radiation was derived from the National Aeronautics and Space Administration/Global Energy and Water Cycle Experiment Surface Radiation Budget, release 3.0 data set (Gupta et al., 2006), the daily averaged precipitation was downloaded from 3B42 Research Derived Daily Product of the Version 7 Tropical Rainfall Measuring Mission Multi-Satellite Precipitation Analysis (Huffman et al., 2010), and the daily averaged 10-m wind speed was obtained from the SeaFlux-V1.0 product.

2.3. PWP Model

To investigate the main process of the annual (semiannual) cycle of wind speed driving the annual (semiannual) cycle of dSST, a series of sensitivity experiments were carried out using the one-dimensional ocean mixed layer model developed by Price et al. (1986, hereafter PWP model). These experiments were divided into three groups (G1, G2, and G3), and each group includes seven experiments (E1, E2, …, and E7) corresponding to different wind speeds. Because the mean wind speed is about 6 m/s and the maximum annual and/or semiannual amplitude of wind speed is about 3 m/s in the SCS, wind speeds corresponding to E1, E2, …, and E7 increase from 3 to 9 m/s. The three groups of experiments were designed as follows:

Table 1
Comparison of Monthly Diurnal Warming of Sea Surface Temperature Derived From the SeaFlux-V1.0 Data Product (the Webster et al. (1996) [W96] Parameterization) With Three ATLAS Buoys in the South China Sea During the Period From April 1998 to March 1999

	18.1°N, 115.6°E	15.3°N, 115.0°E	13.0°N, 114.4°E
Mean (ATLAS)/°C	0.38	0.34	0.38
Mean (SeaFlux)/°C	0.33	0.35	0.36
Mean (W96)/°C	0.41	0.41	0.42
Root-mean-square error (SeaFlux/W96)/°C	0.07/0.09	0.06/0.07	0.07/0.09
Correlation (SeaFlux/W96)	0.93/0.94	0.94/0.96	0.92/0.93

G1: Both wind stress and surface heat loss are different in E1, E2, …, and E7, increasing with wind speed (surface heat loss increases with wind speed linearly. The linear relationship was derived from the OAFLUX data in the SCS using a simple linear regression).

G2: Only wind stress is considered as G1 with same surface heat loss (corresponding to the mean wind speed) in E1, E2, …, and E7.

G3: Only surface heat flux is considered as G1 with same wind stress (corresponding to the mean wind speed) in E1, E2, …, and E7.

In each experiment, water depth is 100 m, and the vertical resolution is 1 m. The initial temperature and salinity profiles are uniform (26 °C and 35 PSU). Each experiment was run using idealized forcing: steady wind stress, steady surface heat loss, and sinusoidal insolation with the maximum value of 700 W/m^2.

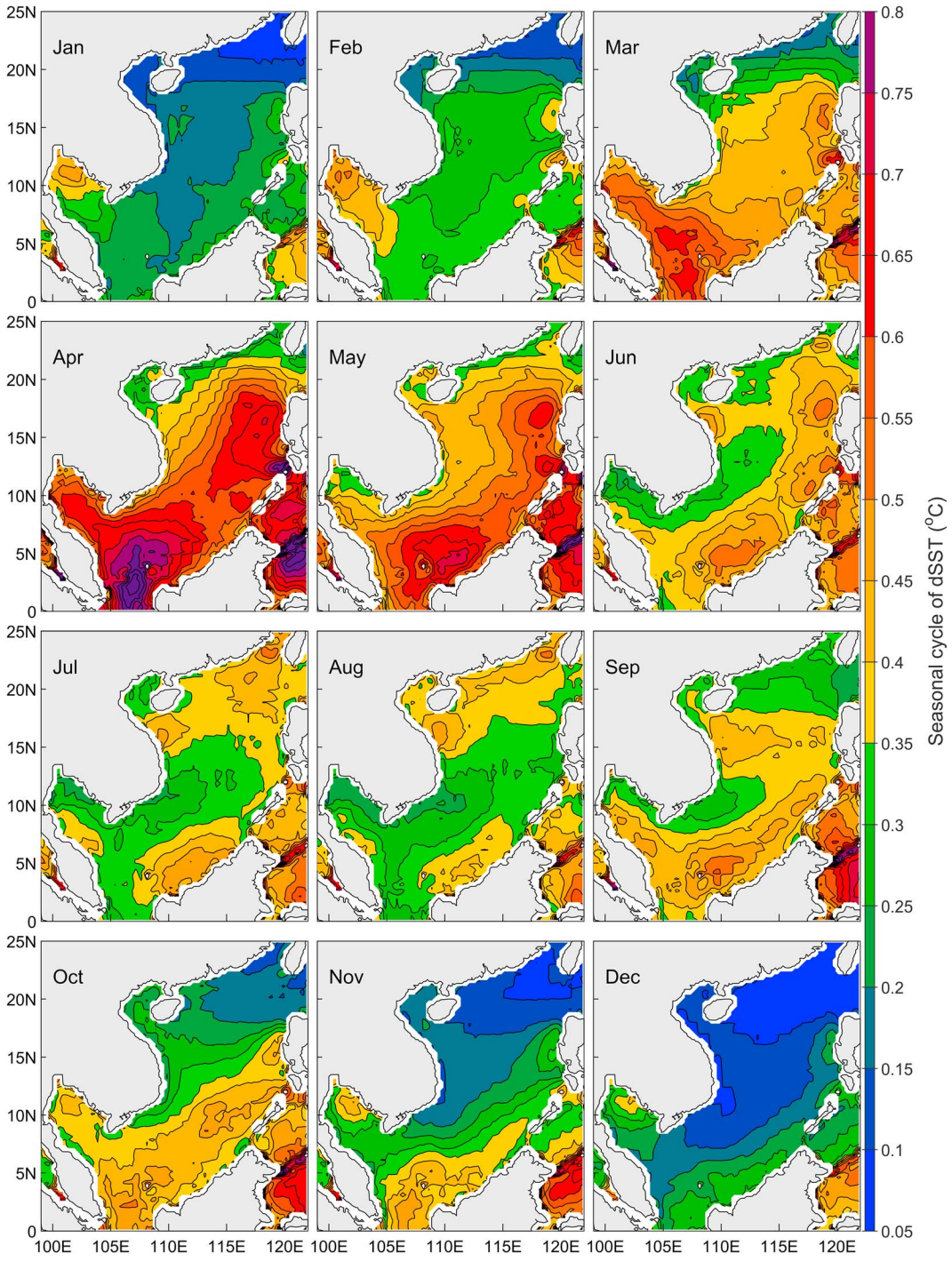

Figure 2. Monthly mean climatological diurnal warming of sea surface temperature (°C) in the South China Sea derived from the SeaFlux data product.

3. Results

3.1. The Annual and Semiannual Cycles of dSST

Figure 2 shows the monthly mean climatological dSST in the SCS. Generally, dSST reaches its minima in December/January and its maxima in April. But dSST in the northern continental shelf has maximum values in July/August. These maps demonstrate an obvious annual signal. In addition, dSST in the central and

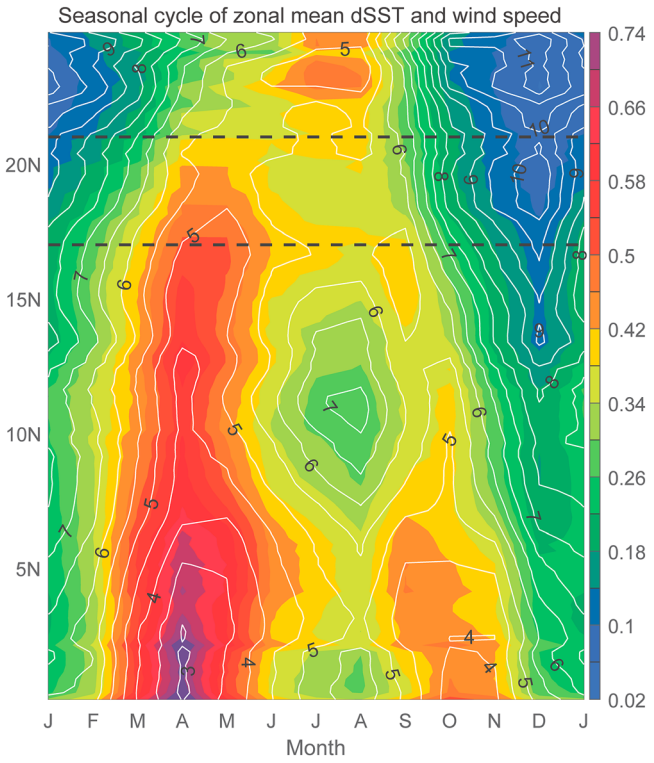

Figure 3. Seasonal cycle of the zonal mean diurnal warming of sea surface temperature (shading, °C) and wind speed (contours, m/s) in the South China Sea. The two dashed lines are at 17°N and 21°N showing the transition lines.

southern SCS forms secondary minima and maxima in August and September/October, respectively, showing a clear semiannual signal. Note that dSST has minimum values in August and secondary minimum values in December in the Gulf of Thailand, opposite to that in the central and southern SCS.

The spatial distribution of the annual and semiannual signals of dSST can also be seen clearly in zonal mean dSST presented in Figure 3. The annual signal is robust north of 17°N with minimum values of dSST in December and maximum values in July/August north of 21°N and in April/May between 17°N and 21°N. The semiannual signal occurs south of 17°N with primary and secondary maximum (minimum) values in April and September/October (December/January and August), respectively.

To directly uncover the annual and semiannual cycles of dSST, harmonic analysis of the dSST time series is conducted (Figure 4). The results show that the amplitude of the dSST annual cycle is greater than 0.1 °C in most areas of the SCS, with a maximum value greater than 0.2 °C located to the west of the Luzon Strait. The annual cycle of dSST reaches its maxima in April/May/June everywhere in the SCS except in the Gulf of Thailand. In comparison, the amplitude of the semiannual cycle of dSST generally increases from north to south with a maximum value greater than 0.2 °C occurring in the Karimata Strait. The timing of the maximum of the semiannual cycle of dSST shifts from February to March along a northwest-southeast axis. Generally, the amplitude of the semiannual cycle is much smaller than that of the annual cycle north of 17°N (ratio $<$ 1/2) and is comparable to or even larger than it south of 17°N (1/2 $<$ ratio $<$ 2) (Figure 4e). This results in the annual signal north of 17°N and the semiannual signal south of 17°N shown in Figure 3.

3.2. Mechanisms Driving the Annual and Semiannual Cycles of dSST

Because the evolution of dSST is mainly driven by wind speed, solar radiation, and precipitation (Webster et al., 1996), the contributions of the annual and semiannual cycles of the three factors are calculated to examine their relative roles as driving mechanisms of the annual and semiannual cycles of dSST in the SCS. Detailed procedure is given in section 2.2. Our calculations suggest that the annual and semiannual cycles of dSST are mainly driven by the associated cycles of solar radiation and wind speed.

For the annual cycle of dSST, the percentage contribution of the annual cycle of wind speed exceeds 50% over most areas of the SCS with largest values occurring along the eastern SCS (whole basin average is 64%, Figure 5a). This suggests that the annual cycle of wind speed makes a primary contribution to the annual cycle of dSST. The contribution of the annual cycle of solar radiation is generally secondary (Figure 5b). Its average percentage contribution in the whole basin is 36%. The spatial distribution is reversed for the annual cycle of solar radiation, where the largest contribution is along the western SCS. In the regions, such as the Beibu Gulf, off the coast of central Vietnam and the southeastern Gulf of Thailand, the contribution of the annual cycle of solar radiation is greater than that of the annual cycle of wind speed. This is due to the relatively small amplitude of the annual cycle in wind speed but the relatively large amplitude annual cycle in solar radiation (Figure 6).

For the semiannual cycle of dSST, the percentage contribution of the semiannual cycle of wind speed generally increases from north to south, and the contribution is greater than that of the semiannual cycle of solar radiation in the SCS except the west of the Luzon Strait (Figures 5c and 5d), where the amplitude of the semiannual cycle of dSST is small (Figure 4c). We conclude that the semiannual cycle of dSST is largely controlled by the semiannual cycle of wind speed.

Figure 7 shows the amplitude and month of the minimum of the semiannual cycle of wind speed. By comparing Figure 7b with Figure 4d, it is clear that the timing of the minimum of the semiannual cycle of

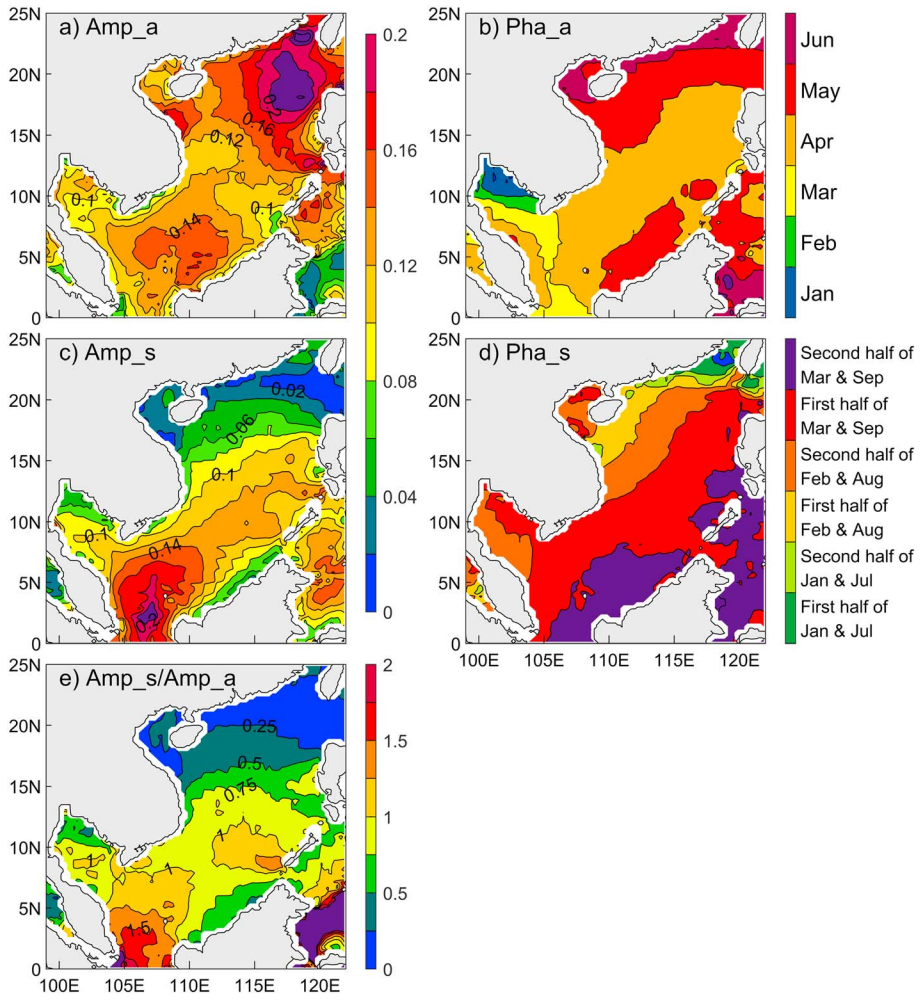

Figure 4. Amplitude and phase (month of the maximum) of the diurnal warming of sea surface temperature (a and b) annual and (c and d) semiannual cycles in the South China Sea. (e) The ratio of the semiannual amplitude to the annual amplitude.

wind speed is nearly coincident with that of the maximum of the semiannual cycle of dSST. However, the spatial pattern of the amplitude of the semiannual wind speed is inconsistent with that of the amplitude of the semiannual cycle in dSST (Figures 7a and 4c). For example, the maximum semiannual amplitude in wind speed is located off southeastern coast of Vietnam, while the maximum in dSST occurs in the Karimata Strait. Kawai and Kawamura (2002) have shown that dSST has a logarithmic dependence on wind speed (dSST~ ln (U)), so dSST change (ΔdSST) induced by wind speed change (ΔU) strongly links with the ratio of the wind speed change to wind speed (ΔdSST~ ln ($U + \Delta U$) $-$ ln (U)~ ln (1 + $\Delta U/U$)). This suggests that the semiannual amplitude of dSST should be proportional to the ratio of the semiannual amplitude of wind speed to the annual mean wind speed. From Figure 7c, this ratio does exhibit a similar pattern to the amplitude of the semiannual cycle of dSST (Figure 4c). These further confirm that the semiannual cycle in wind speed largely controls the semiannual cycle of dSST.

These results suggest that the annual (semiannual) cycle of wind speed is the most important factor for the annual (semiannual) cycle of dSST in the SCS. The strong negative correlation between the seasonal cycle of the zonal mean wind speed and dSST is important evidence supporting this conclusion (Figure 3). This may be explained as follows: In the SCS, the amplitude of the annual (semiannual) cycle in wind speed is relatively large under the control of the East Asian monsoon. However, because the SCS is located in the tropics, the annual (semiannual) cycles in solar radiation are relatively small. Consequently, the annual (semiannual) cycle of wind speed plays the dominant role in the annual (semiannual) cycle of dSST.

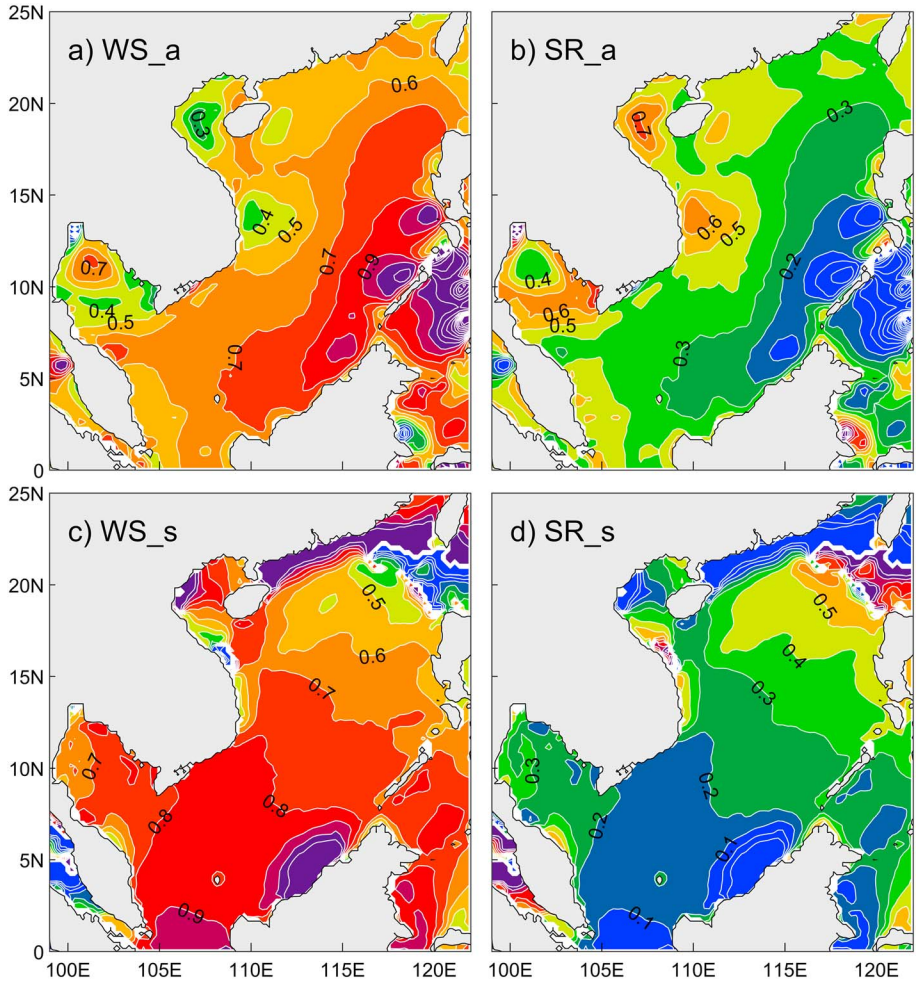

Figure 5. Percentage contributions of the annual cycles of (a) wind speed and (b) solar radiation to the annual cycle of diurnal warming of sea surface temperature. (c and d) The same as a and b except for the semiannual cycle.

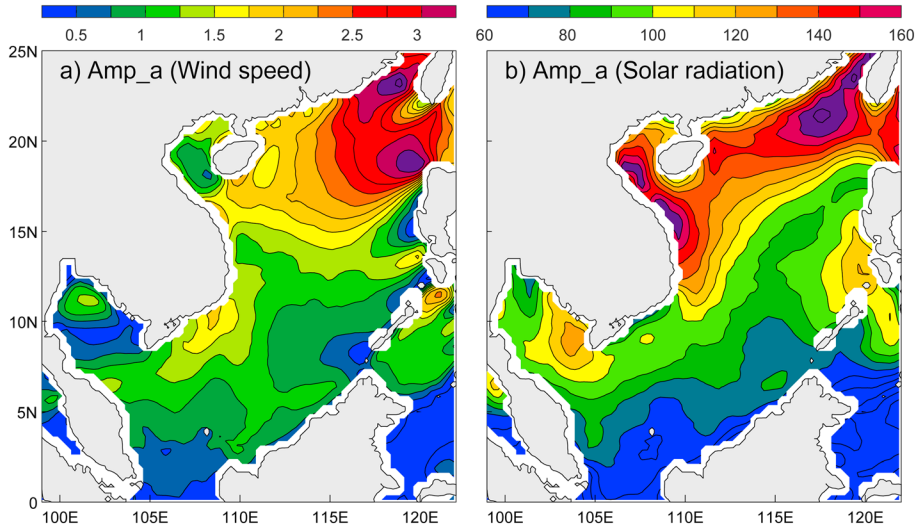

Figure 6. Amplitude of the annual cycles of (a) wind speed (m/s) and (b) peak solar radiation (W/m^2).

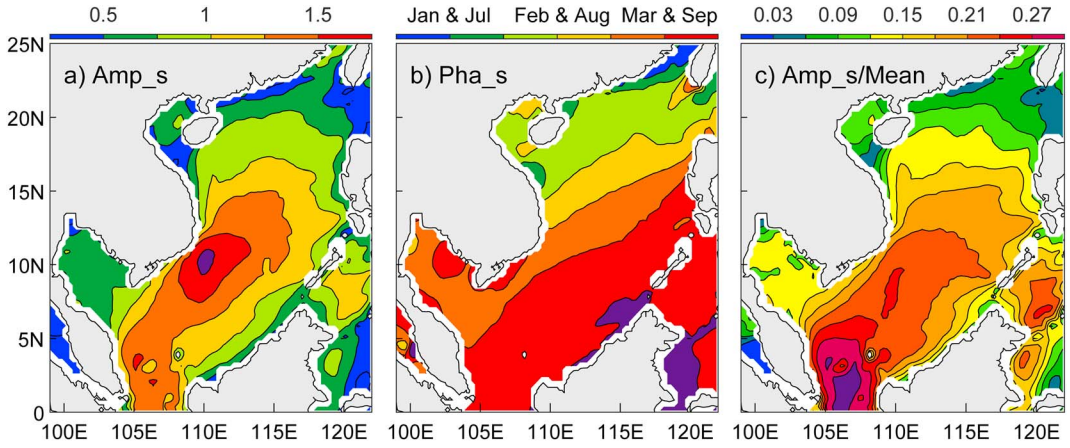

Figure 7. (a) Amplitude (m/s) and (b) phase (month of the minimum) of the semiannual cycle of wind speed in the South Chine Sea. (c) The ratio of the amplitude of the semiannual cycle of wind speed to the annual mean wind speed.

The annual (semiannual) cycle of wind speed drives the annual (semiannual) cycle of dSST by two processes. One is by influencing oceanic vertical turbulent mixing, and the other is by modulating latent and sensible heat flux. To evaluate the relative importance of the two processes, a series of sensitivity experiments with three groups (G1, G2, and G3) were conducted using the PWP model. Detailed configurations are introduced in section 2.3.

In G1, with the increase in wind speed, increased wind stress and increased surface heat loss can increase vertical shear of flow and convective overturning and thereby enhance oceanic vertical turbulent mixing (represented by the mixed layer depth) (Figure 8b) and further decrease dSST (Figure 8a). By comparing the sensitivity experiment results in G1, G2, and G3, it is found that increased wind stress makes a dominated contribution to the decrease of dSST by enhancing oceanic vertical turbulent mixing. From 3 to 9 m/s, increased wind stress (in G2) decreases dSST by 77%, while increased heat loss (in G3) decreases dSST by 13%.

3.3. Mesoscale Features in the Lees of Hills/Islands

Aside from the basin-scale features, both the annual and semiannual cycles of dSST exhibit robust mesoscale features in the lees of hills/islands. For the annual cycle, the occurrence of its maximum changes from April to January in the Gulf of Thailand, which is quite different from the behavior of the rest of the SCS (Figure 4b). By comparison, the semiannual cycle has relatively small amplitude off the coasts of northwestern Borneo and

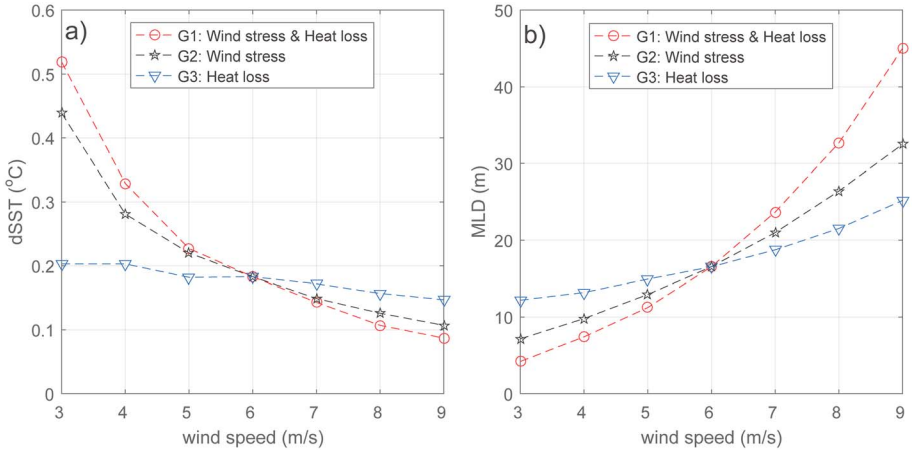

Figure 8. Changes of (a) diurnal warming of sea surface temperature and (b) mixed layer depth with wind speed in the Price et al. (1986) model. In G1, both wind stress and surface heat loss increase with wind speed. In G2, only wind stress increases with wind speed, while only surface heat loss increases with wind speed in G3.

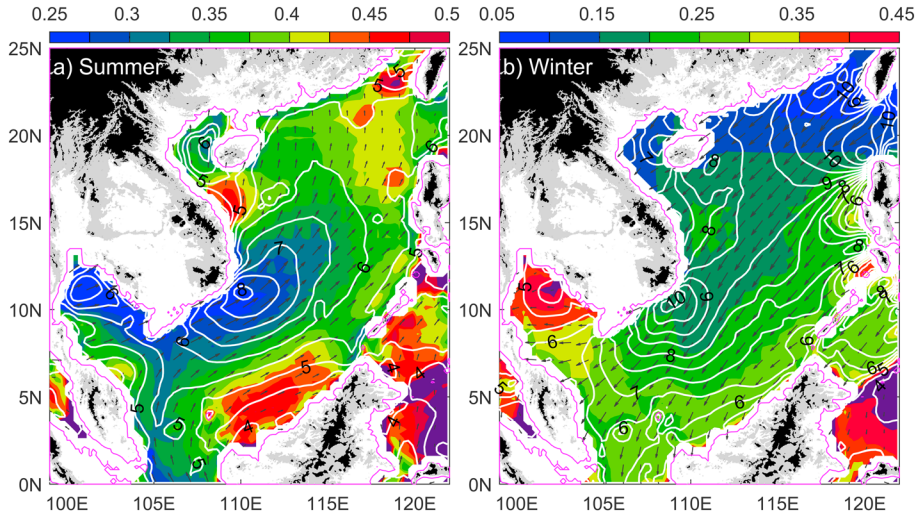

Figure 9. (a) Summer (June–August) and (b) winter (December–January) mean diurnal warming of sea surface temperature (shading, °C), wind speed (contours, m/s), and wind vector (arrows) in the South China Sea. Topographic elevations greater than 200 and 800 m are shaded in gray and black, respectively.

northeastern Vietnam and in the Gulf of Thailand (Figure 4c). These mesoscale features in the lees of hills/islands are a result of sheltering from the monsoon.

Due to orographic sheltering, wind speed is decreased in the lees of hills/islands: off the coasts of northeastern Vietnam, northwestern Borneo, and northeastern Malaysia during the summer monsoon and off the coast of southwestern Taiwan, Luzon, and Mindoro Islands and in the Gulf of Thailand during the winter monsoon (Figure 9) (Li et al., 2014; Wang et al., 2008; Yan et al., 2014). Because of the depression of wind-induced turbulent mixing, dSST increases in the lees of hills/islands (Barton et al., 1998, 2000; Caldeira & Marchesiello, 2002). This effect is especially pronounced off the coasts of northwestern Borneo and northeastern Vietnam and in the Gulf of Thailand (Figure 9). The increased dSST in summer/winter associated with the sheltering from the monsoon weakens the semiannual signal with primary and secondary minimum values in December and August, causing the relatively small amplitude of the semiannual cycle in these three regions (Figure 10). Further, the resulting increase in dSST in the Gulf of Thailand makes it greater in winter than in

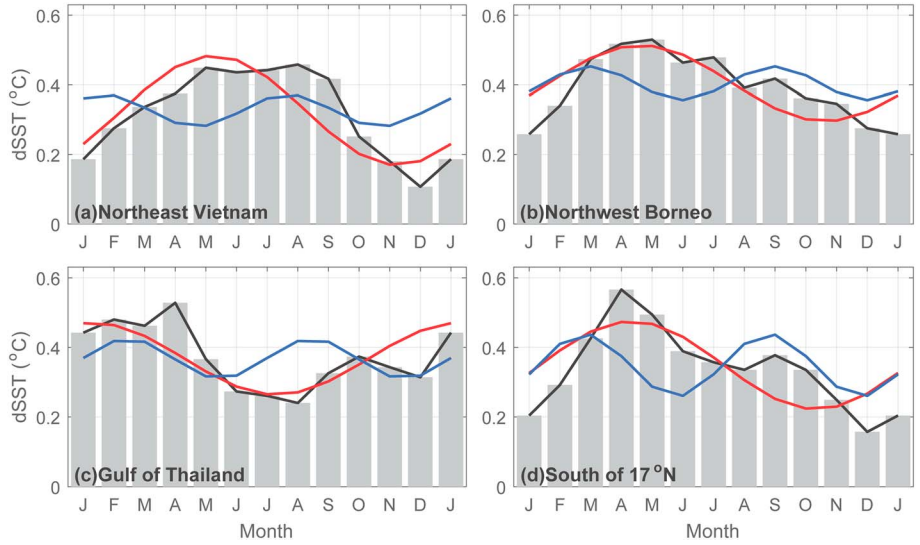

Figure 10. Seasonal (bar and black line), annual (red line), and semiannual (blue line) cycles of diurnal warming of sea surface temperature (°C) (a) off the coast of northeastern Vietnam, (b) off the coast of northwestern Borneo, (c) in the Gulf of Thailand, and (d) in the South China Sea south of 17°N.

summer (Figure 10c). This reverses the dSST situation in the SCS and results in dSST peaking in January in the Gulf of Thailand but in April in the SCS (Figures 10c and 10d).

4. Summary

The annual and semiannual cycles of dSST in the SCS are examined based on the SeaFlux-V1.0 data set, the W96 parameterization, and the PWP model. Harmonic analysis of the time series of dSST shows that the amplitude of the annual cycle is greater than 0.1 °C in most areas of the SCS, and the annual cycle reaches its maxima in April/May/June everywhere in the SCS except in the Gulf of Thailand. The amplitude of the semiannual cycle of dSST in the SCS increases from north to south reaching a maximum value greater than 0.2 °C located in the Karimata Strait. The phase of the semiannual cycle in dSST is such that the month of its maximum changes from February to March along a northwest-southeast axis. Compared with the amplitude of the annual cycle of dSST, the amplitude of the semiannual cycle is much smaller in the area north of 17°N, while it is comparable or even larger south of 17°N. The annual (semiannual) cycle of wind speed is the most important factor for the annual (semiannual) cycle of dSST. The strong negative correlation between the seasonal cycle of the zonal mean wind speed and dSST is important evidence supporting this conclusion. A series of sensitivity experiments demonstrate that the annual (semiannual) cycle of wind speed drives the annual (semiannual) cycle of dSST primarily by changing oceanic vertical turbulent mixing.

Aside from the basin-scale features, both the annual and semiannual cycles of dSST demonstrate robust mesoscale features in the lees of hills/islands as a result of sheltering from the monsoon. Large dSST signals seen in the lees of hills/islands because of the sheltering from the monsoon locally decrease the amplitude of the semiannual cycle of dSST off the coasts of northwestern Borneo and northeastern Vietnam and in the Gulf of Thailand. Further, these effects change the phasing of the annual cycle such that the month of its maximum shifts to January in the Gulf of Thailand.

Acknowledgments
The SeaFlux version 1.0 data product was downloaded from the website: http://seaflux.org/. Solar radiation was derived from the National Aeronautics and Space Administration (NASA)/ Global Energy and Water Cycle Experiment (GEWEX) Surface Radiation Budget (SRB), release 3.0 data set (https://gewex-srb.larc.nasa.gov/). Tropical Rainfall Measuring Mission precipitation data were provided by the Goddard Distributed Active Archive Center (http://trmm.gsfc.nasa.gov/data_dir/data.html). This study is supported by the National Natural Science Foundation of China (grants 41606017, 91428206, 41730536, 41576022, and 41621064), the Program of Shanghai Academic/Technology Research Leader (17XD1400600), the Foundation of Guangdong Province for Outstanding Young Teachers in University (YQ2015088), and the Scientific Research Fund of the Second Institute of Oceanography, SOA (grant 14285).

References

Barton, E. D., Arıstegui, J., Tett, P., Canton, M., Garcıa-Braun, J., Hernandez-Leon, S., & Wild, K. (1998). The transition zone of the Canary Current upwelling region. *Progress in Oceanography*, *41*(4), 455–504. https://doi.org/10.1016/S0079-6611(98)00023-8

Barton, E. D., Basterretxea, G., Flament, P., Mitchelson-Jacob, E. G., Jones, B., Arıstegui, J., & Herrera, F. (2000). Lee region of Gran Canaria. *Journal of Geophysical Research*, *105*(C7), 17,173–17,193. https://doi.org/10.1029/2000JC900010

Bernie, D., Guilyardi, E., Madec, G., Slingo, J., Woolnough, S., & Cole, J. (2008). Impact of resolving the diurnal cycle in an ocean-atmosphere GCM. Part 2: A diurnally coupled CGCM. *Climate Dynamics*, *31*(7-8), 909–925. https://doi.org/10.1007/s00382-008-0429-z

Bernie, D., Woolnough, S., Slingo, J., & Guilyardi, E. (2005). Modeling diurnal and intraseasonal variability of the ocean mixed layer. *Journal of Climate*, *18*(8), 1190–1202. https://doi.org/10.1175/JCLI3319.1

Caldeira, R., & Marchesiello, P. (2002). Ocean response to wind sheltering in the Southern California Bight. *Geophysical Research Letters*, *29*(13), 1635. https://doi.org/10.1029/2001GL014563

Clayson, C. A., & Bogdanoff, A. S. (2013). The effect of diurnal sea surface temperature warming on climatological air-sea fluxes. *Journal of Climate*, *26*(8), 2546–2556. https://doi.org/10.1175/JCLI-D-12-00062.1

Clayson, C. A., & Curry, J. A. (1996). Determination of surface turbulent fluxes for the Tropical Ocean-Global Atmosphere Coupled Ocean-Atmosphere Response Experiment: Comparison of satellite retrievals and in situ measurements. *Journal of Geophysical Research*, *101*(C12), 28,515–28,528. https://doi.org/10.1029/96JC02022

Clayson, C. A., & Weitlich, D. (2005). Diurnal warming in the tropical Pacific and its interannual variability. *Geophysical Research Letters*, *32*, L21604. https://doi.org/10.1029/2005GL023786

Clayson, C. A., & Weitlich, D. (2007). Variability of tropical diurnal sea surface temperature. *Journal of Climate*, *20*(2), 334–352. https://doi.org/10.1175/JCLI3999.1

Gentemann, C. L., & Minnett, P. J. (2008). Radiometric measurements of ocean surface thermal variability. *Journal of Geophysical Research*, *113*, C08017. https://doi.org/10.1029/2007JC004540

Gentemann, C. L., Minnett, P. J., Le Borgne, P., & Merchant, C. J. (2008). Multi-satellite measurements of large diurnal warming events. *Geophysical Research Letters*, *35*, L22602. https://doi.org/10.1029/2008GL035730

Guemas, V., Salas-Melia, D., Kageyama, M., Giordani, H., & Voldoire, A. (2011). Impact of the ocean mixed layer diurnal variations on the intraseasonal variability of sea surface temperatures in the Atlantic Ocean. *Journal of Climate*, *24*(12), 2889–2914. https://doi.org/10.1175/2010JCLI3660.1

Gupta, S. K., Stackhouse, P. W. Jr., Cox, S. J., Mikovitz, J. C., & Zhang, T. (2006). Surface Radiation Budget project completes 22-year data set. In *GEWEX news*, no. 6 (4), (pp. 12–13). silver spring, MD: international GEWEX project office.

Huffman, G. J., Adler, R. F., Bolvin, D. T., & Nelkin, E. J. (2010). The TRMM Multi-Satellite Precipitation Analysis (TMPA). *Journal of Hydrometeorology*, *90*(3), 237–247. https://doi.org/10.1007/978-90-481-2915-7_1

Kawai, Y., & Kawamura, H. (2002). Evaluation of the diurnal warming of sea surface temperature using satellite-derived marine meteorological data. *Journal of Oceanography*, *58*(6), 805–814. https://doi.org/10.1023/A:1022867028876

Kawai, Y., & Kawamura, H. (2005). Spatial and temporal variations of model-derived diurnal amplitude of sea surface temperature in the western Pacific Ocean. *Journal of Geophysical Research*, *110*, C08012. https://doi.org/10.1029/2004JC002652

Kawai, Y., & Wada, A. (2007). Diurnal Sea surface temperature variation and its impact on the atmosphere and ocean: A review. *Journal of Oceanography*, *63*(5), 721–744. https://doi.org/10.1007/s10872-007-0063-0

Kennedy, J. J., Brohan, P., & Tett, S. F. B. (2007). A global climatology of the diurnal variations in sea-surface temperature and implications for MSU temperature trends. *Geophysical Research Letters*, *34*, L05712. https://doi.org/10.1029/2006GL028920

Kettle, H., Merchant, C. J., Jeffery, C. D., Filipiak, M. J., & Gentemann, C. L. (2009). The impact of diurnal variability in sea surface temperature on the Central Atlantic air-sea CO2 flux. *Atmospheric Chemistry and Physics*, *9*(2), 529–541. https://doi.org/10.5194/acp-9-529-2009

Lau, K. M., Ding, Y. H., Wang, J.-T., Johnson, R., Keenan, T., Cifelli, R., et al. (2000). A report of the field operations and early results of the South China Sea monsoon experiment (SCSMEX). *Bulletin of the American Meteorological Society*, *81*(6), 1261–1270. https://doi.org/10.1175/1520-0477(2000)081<1261:AROTFO>2.3.CO;2

Li, J. X., Zhang, R., Ling, Z., Bo, W., & Liu, Y. (2014). Effects of Cardamom Mountains on the formation of the winter warm pool in the Gulf of Thailand. *Continental Shelf Research*, *91*, 211–219. https://doi.org/10.1016/j.csr.2014.10.001

Li, Y., Han, W., Shinoda, T., Wang, C., Liena, R.-C., Moum, J. N., & Wang, J.-W. (2013). Effects of the diurnal cycle in solar radiation on the tropical Indian Ocean mixed layer variability during wintertime Madden-Julian Oscillations. *Journal of Geophysical Research: Oceans*, *118*, 4945–4964. https://doi.org/10.1002/jgrc.20395

Lin, R., Zhang, C. Y., & Li, Y. (2011). Satellite observation of the temporal and spatial variation of sea surface diurnal warming in the South China Sea [in Chinese]. *Journal of Tropical Oceanography*, *33*(2), 17–27. https://doi.org/10.3969/j.issn.1009-5470.2014.02.003

Lv, K. W., Hu, J. Y., & Yang, X. Y. (2012). Spatial patterns in seasonal variability of sea surface wind over the South China Sea and its adjacent ocean. *Journal of Tropical Oceanography* [in Chinese], *31*(6), 41–47. https://doi.org/10.3969/j.issn.1009-5470.2012.06.007

Marullo, S., Minnett, P. J., Santoleri, R., & Tonani, M. (2016). The diurnal cycle of sea-surface temperature and estimation of the heat budget of the Mediterranean Sea. *Journal of Geophysical Research: Oceans*, *121*, 8351–8367. https://doi.org/10.1002/2016JC012192

Price, J. F., Weller, R. A., & Pinkel, R. (1986). Diurnal cycling: Observations and models of the upper ocean response to diurnal heating, cooling, and wind mixing. *Journal of Geophysical Research*, *91*(C7), 8411–8427. https://doi.org/10.1029/JC091iC07p08411

Shinoda, T., Hendon, H. H., & Glick, J. (1998). Intraseasonal variability of surface fluxes and sea surface temperature in the tropical western Pacific and Indian Oceans. *Journal of Climate*, *11*(7), 1685–1702. https://doi.org/10.1175/1520-0442(1998)011,2668:MLMOIV.2.0.CO;2

Stuart-Menteth, A., Robinson, I. S., & Challenor, P. G. (2003). A global study of diurnal warming using satellite-derived sea surface temperature. *Journal of Geophysical Research*, *108*(C5), 3155. https://doi.org/10.1029/2002JC001534

Tu, Q. G., Pan D. L., Hao Z. Z., & Chen J. Y. (2015), Observations of SST diurnal variability in the South China Sea, SPIE Remote Sensing (Vol. 9638, pp.96380O).

Tu, Q. G., Pan, D. L., Hao, Z. Z., & Yan, Y. W. (2016). SST diurnal warming in the China seas and northwestern Pacific Ocean using MTSAT satellite observations. *Acta Oceanologica Sinica*, *35*(12), 12–18. https://doi.org/10.1007/s13131-016-0968-9

Wang, G., Chen, D., & Su, J. (2008). Winter eddy genesis in the eastern South China Sea due to orographic wind jets. *Journal of Physical Oceanography*, *38*(3), 726–732. https://doi.org/10.1175/2007JPO3868.1

Ward, B. (2006). Near-surface ocean temperature. *Journal of Geophysical Research*, *111*, C02005. https://doi.org/10.1029/2004JC002689

Webster, P. J., Clayson, C. A., & Curry, J. A. (1996). Clouds, radiation, and the diurnal cycle of sea surface temperature in the tropical Western Pacific. *Journal of Climate*, *9*(8), 1712–1730. https://doi.org/10.1175/1520-0442(1996)009<1712:CRATDC>2.0.CO;2

Weihs, R., & Bourassa, M. (2014). Modeled diurnally varying sea surface temperatures and their influence on surface heat fluxes. *Journal of Geophysical Research: Oceans*, *119*, 4101–4123. https://doi.org/10.1002/2013JC009489

Xie, S.-P., Xie, Q., Wang, D., & Liu, W. T. (2003). Summer upwelling in the South China Sea and its role in regional climate variations. *Journal of Geophysical Research*, *108*(C8), 3261. https://doi.org/10.1029/2003JC001867

Yan, Y. W., Chen, C. L., & Ling, Z. (2014). Warm water wake off Northeast Vietnam in the South China Sea. *Acta Oceanologica Sinica*, *33*(11), 55–63. https://doi.org/10.1007/s13131-014-0555-x